

Atomic and electronic structures of p-type dopants in 4H-SiC

Lingyan Lu(卢玲燕), Han Zhang(张涵), Xiaowei Wu(吴晓维), Jing Shi(石晶), and Yi-Yang Sun(孙宜阳)

Citation: Chin. Phys. B, 2021, 30 (**9**): 096806. DOI: 10.1088/1674-1056/ac1e22
Journal homepage: http://cpb.iphy.ac.cn; http://iopscience.iop.org/cpb

What follows is a list of articles you may be interested in

Adsorption and rotational barrier for a single azobenzene molecule on Au(111) surface

Dong Hao(郝东), Xiangqian Tang(唐向前), Wenyu Wang(王文宇), Yang An(安旸), Yueyi Wang(王悦毅), Xinyan Shan(单欣岩), and Xinghua Lu(陆兴华)

Chin. Phys. B, 2021, 30 (**9**): 096805. DOI: 10.1088/1674-1056/ac11d9

NBN-doped nanographene embedded with five- and seven-membered rings on Au(111) surface

Huan Yang(杨欢), Yun Cao(曹云), Yixuan Gao(高艺璇), Yubin Fu(付钰彬), Li Huang(黄立), Junzhi Liu(刘俊治), Xinliang Feng(冯新亮), Shixuan Du(杜世萱), and Hong-Jun Gao(高鸿钧)

Chin. Phys. B, 2021, 30 (**5**): 056802. DOI: 10.1088/1674-1056/abeede

Super-strong interactions between multivalent anions and graphene

Xing Liu(刘星) and Guosheng Shi(石国升)

Chin. Phys. B, 2021, 30 (**4**): 046801. DOI: 10.1088/1674-1056/abd396

First-principles study of high performance lithium/sodium storage of $Ti_3C_2T_2$ nanosheets as electrode materials

Li-Na Bai(白丽娜), Ling-Ying Kong(孔令莹), Jing Wen(温静), Ning Ma(马宁), Hong Gao(高红), Xi-Tian Zhang(张喜田)

Chin. Phys. B, 2020, 29 (**1**): 016802. DOI: 10.1088/1674-1056/ab592e

Interface effect on structural and electronic properties of graphdiyne adsorbed on SiO_2 and h-BN substrates: A first-principles study

Dong Bao-Juan, Yang Teng, Wang Ji-Zhang, Zhang Zhi-Dong

Chin. Phys. B, 2015, 24 (**9**): 096806. DOI: 10.1088/1674-1056/24/9/096806

Atomic and electronic structures of p-type dopants in 4H-SiC

Lingyan Lu(卢玲燕)[1,†], Han Zhang(张涵)[2,†], Xiaowei Wu(吴晓维)[2], Jing Shi(石晶)[1,‡], and Yi-Yang Sun(孙宜阳)[2,§]

[1] *Department of Physics, Jiangxi Normal University, Nanchang* 330022, *China*

[2] *State Key Laboratory of High Performance Ceramics and Superfine Microstructure, Shanghai Institute of Ceramics, Chinese Academy of Sciences, Shanghai* 201899, *China*

(Received 7 July 2021; revised manuscript received 26 July 2021; accepted manuscript online 17 August 2021)

Using hybrid density functional calculation, we study the atomic and electronic structures of p-type dopants, B, Al and Ga, in 4H-SiC. For B, depending on the growth condition, it can occupy both Si and C sites. In contrast, Al and Ga on the C sites exhibit too high formation energy to exist in a significant amount. In 4H-SiC, there exist two types of Si sites in wurtzite-like and zincblende-like local coordination, respectively. Our calculations suggest that the dopant atoms have negligible preference occupying the two sites. In neutral charge state, all the dopants exhibit significant distortions from the structure in the negatively charged state. For most cases, our calculations yield three distorted structures, in which the most stable one has the dopant atom displaced along its bond with one of the surrounding equatorial Si or C atoms, lowering the C_{3v} symmetry to C_s symmetry (i.e., a mirror symmetry only). Among the three dopant elements, Al on Si sites exhibits overall the lowest formation energy and the shallowest acceptor level. Nevertheless, it is not a hydrogenic dopant with the acceptor level 0.12 eV above the valence band maximum based on calculation using a 400-atom supercell. Its corresponding defect state exhibits apparent localization along the [0001] direction, but it is relatively delocalized in the (0001) plane.

Keywords: wide band gap semiconductors, p-type doping, SiC, density functional theory

PACS: 68.55.Ln, 71.15.Mb **DOI:** 10.1088/1674-1056/ac1e22

1. Introduction

Power electronic devices have found more and more applications in our everyday life, including fast-chargers for mobile electronic devices, inverters for electricity generation by solar and wind energy, electric cars and trains, just to name a few. Silicon-based devices are becoming more and more mature. Meanwhile, they are also approaching the limits of device specifications, in particular, breakdown voltage. To meet the market demands on high working voltage, as well as on device miniaturization, wide-band-gap semiconductors have been proposed for power electronics.[1] Generally, the breakdown voltage is proportional to the band gap.[2] Even though many wide-band-gap semiconductors have been explored, silicon carbide (SiC) and gallium nitride (GaN) are currently the two most successful materials. A key barrier for discovering new power electronic materials is bipolar doping for making p–n junctions. By far, SiC and GaN are the only two materials that can be sufficiently doped to both n- and p-types among semiconductors with the band gap greater than 3 eV.[3,4] Except for rare cases, such as diamond, p-type doping is usually more difficult than n-type doping.[5]

SiC and GaN have large band gaps of 3.27 eV and 3.50 eV, respectively.[6,7] As a result, both of them exhibit a high breakdown field of 3–4 MV/cm,[8,9] an order of magnitude higher than that of silicon. In comparison, SiC has a thermal conductivity of about 4.7 $W\cdot cm^{-1}\cdot K^{-1}$ at room temperature, significantly higher than that of GaN[10,11] and therefore, is more favored for high-power and high-temperature applications. On the other hand, GaN exhibits high electron mobility of 2000 $cm^2\cdot V^{-1}\cdot s^{-1}$, significantly higher than that of SiC.[12,13] The values quoted above are for 4H-SiC, which is one of the numerous polymorphs of SiC and most favored for power electronic devices by overall consideration on electron mobility, breakdown field, thermodynamic stability, etc.[14]

Trivalent elements (B, Al and Ga) are the choice of p-type dopants for SiC. Currently, Al is the most commonly adopted in making power electronic devices. However, Al in SiC is not a sufficiently shallow acceptor. Its acceptor level is experimentally reported to be 0.22 eV or greater,[15] rendering the p-type doping still an issue in device fabrication. A number of theoretical studies reported atomic and electronic structures of p-type dopants in different polymorphs of SiC.[16–19] However, a key structural feature, namely, off-center displacement of the dopant atom, has been missed until recently a hybrid density functional was adopted in the calculation.[20] Such distortion by breaking the local C_{3v} symmetry to a C_{1h} (or C_s) point-group symmetry has been noticed in an earlier work.[21] Such distortions are also known for other wide-band-gap semiconductors, such as ZnO and GaN.[22]

In this paper, we study the atomic and electronic structures of group-III elements (B, Al and Ga) in 4H-SiC based on

†These authors contributed equally.

‡Corresponding author. E-mail: sjd865@jxnu.edu.cn

§Corresponding author. E-mail: yysun@mail.sic.ac.cn

© 2021 Chinese Physical Society and IOP Publishing Ltd

hybrid density functional calculations. We consider the possibility of dopants on Si and C sites and for both cases we consider the wurtzite-like (wz) and zincblende-like (zb) sites. We also study the possible off-center distortions and determine the stable and metastable structures for these p-type dopants. Employing chemical potentials for all elements in our defect formation calculations, we study the effect of secondary phases on the doping. We compare the acceptor levels of the group-III elements in 4H-SiC at all possible local structures, which determine the doping efficiency and may provide a useful guide in the future dopant engineering in 4H-SiC.

2. Computational method

Our calculations were based on density functional theory (DFT) implemented in Vienna *ab initio* simulation (VASP) package,[23] which describes the interaction between the ion-cores and valence electrons by projector augmented wave (PAW) potentials.[24] Plane waves with cutoff energy of 30 Ry were taken as the basis set. We used the hybrid exchange-correlation functional of Heyd, Scuseria and Ernzerhof (HSE),[25] which includes 25% of Hartree–Fock exchange energy with its long-range part removed by using the error function. The supercell method was used to model the defects. A $4\times4\times1$ (128-atom) supercell and a $5\times5\times2$ (400-atom) supercell were used in our calculations. The Γ point was used to represent the Brillouin zone of the defect supercells. All calculations on neutral defects, which exhibit a spin magnetic moment of 1 μ_B, were spin-polarized. The atomic structures were fully relaxed until the calculated forces on all atoms were less than 0.5 mRy/Bohr. When optimizing the lattice constants, we used a cutoff energy of 45 Ry and a $5\times5\times2$ Monkhorst–Pack k-point grid, which yielded $a = 3.071$ Å and $c = 10.043$ Å.

3. Results and discussion

Figure 1(a) shows the atomic structure of 4H-SiC from a side view. Each unit cell contains four Si layers and four C layers along the [0001] direction. Aided by the two red-color guiding lines, it can be seen that two of the Si layers have their local coordination environment similar to that in the wurtzite structure and another two similar to that in the zincblende structure. The two different sites are referred to as Si_{wz} and Si_{zb}, respectively, in this paper. The C sites are labelled similarly as C_{wz} and C_{zb}, respectively.

Figure 1(b) shows the calculated band structure of 4H-SiC using the HSE functional. The valence band maximum (VBM) is located at the Γ point and the conduction band minimum (CBM) is located at the M point. The band gap is calculated to be 3.17 eV, in reasonable agreement with the experimental value.[6] The calculated electron effective masses along the M–Γ and M–K directions are $0.54m_0$ and $0.30m_0$, respectively, which are comparable with the measured values of $0.42m_0$ and $0.29m_0$ [26,27] In comparison, the hole effective masses of $2.77m_0$, $1.82m_0$ and $1.52m_0$ along the Γ–M, Γ–K, and Γ–A directions, respectively, are significantly larger than those of electrons.

Next, we investigate the properties of p-type dopants (B, Al and Ga) in 4H-SiC. To study the atomic structures, we follow a procedure shown in Fig. 2(a). First, we consider whether the dopant atoms occupy the Si or the C sites. Initiatively, B has an ionic radius close to C suggesting that it may favor the C sites, while Al and Ga may favor the Si sites due to the larger ionic radii. To quantify these arguments, the defect formation energy needs to be calculated. Second, as shown in Fig. 1(a),

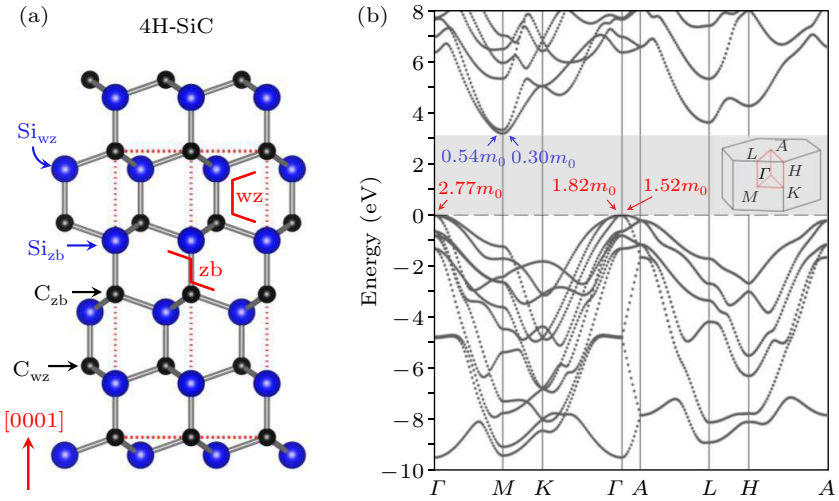


Fig. 1. (a) Atomic structure of 4H-SiC from a side view. The red dashed frame marks the unit cell, which contains four Si layers and four C layers along the [0001] direction. The two red solid lines guide the eye to identify the wurtzite (wz) and zincblende (zb) local coordination for two different Si sites, referred to as Si_{wz} and Si_{zb}, respectively, The C sites are labeled similarly as C_{wz} and C_{zb}, respectively. (b) Band structure of 4H-SiC calculated using the HSE functional. The gray region is the band gap. The electron effective masses along three directions and the hole effective masses along two directions are shown in the inset. The first Brillouin zone and the high-symmetry k-points are also shown in the inset.

4H-SiC exhibits two different sites for both Si and C atoms. It is necessary to study the occupation preference between the two sites. Third, it is relatively less discussed in the literature that these p-type dopants undergo significant distortion in the neutral charge state, referred to as defect-bound small polarons.[28]

Figure 2(b) shows the possible distortion directions. By taking a Si-site dopant (denoted by D) as an example, C_0 is the axial C atom with the C_0–D bond parallel to the [0001] direction. C_1, C_2 and C_3 are the three equatorial C atoms. In the figure, C_2 and C_3 are overlapped with each other. If the D atom is displaced along the C_0–D bond, the local C_{3v} point-group symmetry is preserved with two possible directions marked by Δ_2 and Δ_2' in Fig. 2(b). If the D atom is displaced along the C_1–D bond, then the C_{3v} symmetry is broken and only a mirror passing C_1, C_0 and the middle point between C_2 and C_3 is maintained, i.e., C_s (or C_{1h}) point-group symmetry. This type of distortions is marked by Δ_1 and Δ_1' in Fig. 2(b). The third type of distortions, marked by Δ_3 and Δ_3', also maintain the C_s symmetry only with the displacement direction of the D atom bisecting the C_2–D–C_3 angle.

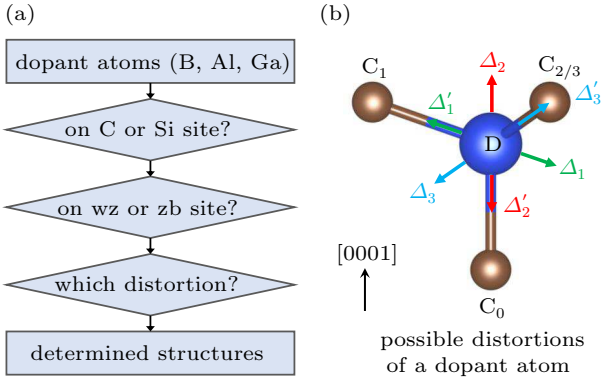


Fig. 2. (a) Flow chart for determining the atomic structure of group-III dopants in 4H-SiC, including the preferences on Si or C sites and on wurtzite-like (wz) or zincblende-like (zb) sites, as well as the distortions of the dopant atoms. (b) Possible distortions of a dopant atom (denoted by D) on a Si site. C_0 is the axial C atom with the C_0–D bond parallel to the [0001] direction. C_1, C_2 and C_3 are the three equatorial C atoms surrounding the Si site, where C_2 and C_3 are overlapped with each other. There are three possible types of displacements for the D atom. Δ_1 is along the C_1–D bond, Δ_2 is along the C_0–D bond, and Δ_3 is along the direction bisecting the C_2–D–C_3 angle. Each of them can have an opposite direction, marked by a prime.

The defect formation energies were calculated according to $\Delta H(\{\mu_i\}, E_F, q) = E_D(q) - E_0 + \sum_i n_i(E_i + \mu_i) + q(E_{VBM} + E_F)$, where $E_D(q)$ is the total energy of the defect supercell in charge q, E_0 is the total energy of the perfect supercell and $\{\mu_i\}$ are the chemical potentials. The detailed description for each term can be found in our previous work.[29] We first adopted the 128-atom supercell. To determine the allowed range for the chemical potentials $\{\mu_i\}$, it is required to satisfy $\mu_{Si} + \mu_C = \Delta H$ (4H-SiC), which is the enthalpy of formation of 4H-SiC. Also, successful doping needs to avoid the formation of secondary phases. B tends to form B_4C [30] and B_3Si [31] and Al tends to form Al_4C_3,[32] while Ga does not form stable compounds with either Si or C. For each secondary phase, the sum of $\{\mu_i\}$ with corresponding weights needs to be lower than the enthalpy of formation of that phase. The conditions to satisfy are shown in Fig. 3(a) with the values of formation enthalpy for each secondary phase calculated by the HSE functional.

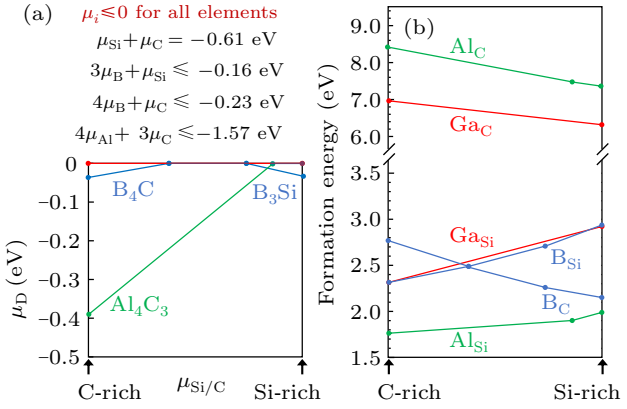


Fig. 3. (a) Determination of chemical potentials for the dopant elements (μ_D) between C-rich ($\mu_C = 0$) and Si-rich ($\mu_{Si} = 0$) conditions. μ_B (blue line) is limited by the formation of B_4C and B_3Si. μ_{Al} (green line) is limited by the formation of Al_4C_3. μ_{Ga} (red line) can be constantly 0 (i.e., Ga-rich). The conditions to satisfy are shown above the plot. All enthalpies of formation are calculated by the HSE functional. (b) Formation energy of B, Al and Ga on Si and C sites calculated by the HSE functional. For B and Al, the lines are segmented because the chemical potentials of B and Al are segmented as shown in (a).

From Fig. 3(a) it can be seen that μ_{Ga} can be constantly 0 (red line), meaning that the growth condition for doping Ga can be Ga-rich and there is no need to consider the formation of secondary phases. For B, due to the formation of B_4C and B_3Si under C- and Si-rich conditions, respectively, the growth condition for doping B cannot be overly B-rich. Nevertheless, because the ΔH for the two B-induced secondary phases are small, their effect on the defect formation energy is relatively small. In comparison, the formation of Al_4C_3 limits μ_{Al} to be below -0.39 eV under C-rich condition, which is the favored growth condition for Al occupying Si sites.

Figure 3(b) shows that Al and Ga on C sites have high formation energies above 6 eV suggesting that it is almost impossible to have Al and Ga to occupy C sites in a significant amount. They will not be considered below. Our results show that B can occupy both Si and C sites depending on the growth condition. Under C-rich condition, B tends to occupy the Si sites, while under Si-rich condition, B tends to occupy the C sites. Even though the Al-rich condition is limited by the formation of Al_4C_3 as mentioned above, Al on Si site still exhibits the lowest formation energy, about 1.77 eV at C-rich (or Si-poor) condition for neutral charge state.

Regarding the site preference between the wz and zb sites, our calculations show that the energy difference on the two sites is small, less than 10 meV for the two Si sites. For the two C sites, B on the C_{zb} site is more stable than on the C_{wz}

site by 16 meV. For typical growth temperature of 4H-SiC, this small energy would not result in significant occupation preference.

We next discuss the distortions. It is more convenient to discuss the stability of the distortions together with the calculated acceptor level (or ionization energy), which is obtained by $\varepsilon(0/-) = E_{\rm D}(-) - E_{\rm D}(0) - E_{\rm VBM}$. Because the defects do not show different distortions in the 1− charge state, a less stable structure in the neutral charge by having a higher $E_{\rm D}(0)$ will yield a lower (or shallower) acceptor level $\varepsilon(0/-)$. Figure 4(a) shows the calculated $\varepsilon(0/-)$ levels for B on both the Si and C sites and Al/Ga on the Si sites. For each case, we consider the occupation preference between the wz and zb sites, which ends up with eight defects. For each defect, we find three relaxed structures.

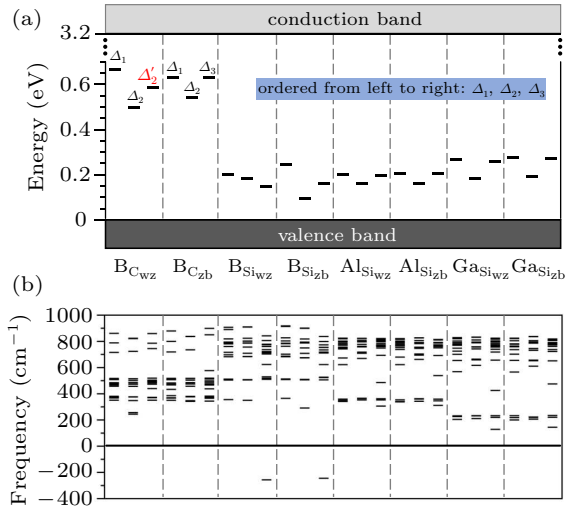


Fig. 4. (a) Calculated acceptor levels (or ionization energy), $\varepsilon(0/-)$, for B, Al, and Ga on Si and C sites using the 128-atom supercell. Because Al and Ga have high formation energies on the C sites, they are not considered here. For each defect, results for three distortions are shown. They are arranged as Δ_1, Δ_2, and Δ_3 from left to right with one exception for B on C_{wz} site, for which the Δ_3 distortion was not found and instead the Δ_2' distortion is shown. (b) Calculated vibrational frequencies by allowing the dopant atom and the four surrounding Si or C atoms to move, while fixing all other atoms in the supercell. HSE functional was used in all frequency calculations.

As shown in Fig. 4(a), most of the relaxed structures exhibit the Δ_1, Δ_2, and Δ_3 distortions, as illustrated in Fig. 2(b). There is one exception, B on C_{wz} site, for which we found that Δ_2' is a stable distortion, while Δ_3 is unstable. The Δ_1 distortion is always the most stable one and gives rise to the deepest $\varepsilon(0/-)$ level. For most cases, the Δ_3 distortion is the second stable one. The Δ_2 distortion preserving the C_{3v} symmetry is the least stable one. There is one exception, B on Si_{wz} site, for which the Δ_3 distortion is the least stable one. Experimentally, it was found that Al acceptors exhibit two ionization levels.[15] According to our results, different distorted structures may be responsible for the experimental observations if the nearly degenerate Δ_1 and Δ_3 distortions correspond to one ionization level and the Δ_2 distortion corresponds to the other one.

To further confirm whether all the distortions shown in Fig. 4(a) are stable structures, we carried out frequency calculations. We allowed the dopant atom and its surrounding four Si or C atoms to move, while fixing all other atoms in the supercell. All these calculations were also based on the HSE functional keeping all calculation parameters the same as those when relaxing the structures. The results are shown in Fig. 4(b). It can be seen that most of them are indeed stable or metastable. Only the Δ_3 distortions for B on the two Si sites exhibit imaginary frequencies suggesting that they are unstable. It is noted that if one simply relaxes the structure by replacing a Si or C with the dopant atom in neutral charge state, but does not initially displace the dopant atom following the directions in Fig. 2(b), the obtained structures are always unstable and exhibit one or more imaginaries frequencies.

From Fig. 4(a) it can be seen that all p-type dopants in 4H-SiC show relatively deep $\varepsilon(0/-)$ levels of above 0.2 eV. Because the calculations on $\varepsilon(0/-)$ is subject to the supercell size effect, we further checked the results by using a 400-atom supercell. Figure 5(a) shows that using the large supercell, the $\varepsilon(0/-)$ levels all become shallower than those obtained using the 128-atom supercell, especially for the cases of Al and Ga. It becomes clear that Al exhibits the shallowest $\varepsilon(0/-)$ levels and the wz and zb sites do not have significant difference.

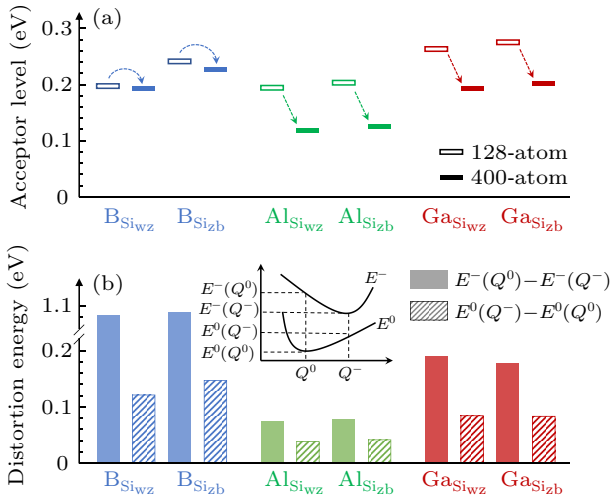


Fig. 5. (a) Comparison of the $\varepsilon(0/-)$ levels calculated using the 128-atom and 400-atom supercells. (b) Distortion energies calculated using the 400-atom supercell between the relaxed structures in the neutral and 1− charge states, denoted by Q^0 and Q^-, respectively. The distortion energies between the two structures in the neutral (E^0) and 1− (E^-) charge states are different and shown by shaded and filled bars, respectively. The inset illustrates the involved quantities. For all defects, the most stable Δ_1 distortions were used.

Table 1 shows the comparison of the relaxed bond lengths from the 128-atom and 400-atom supercells. For the Δ_1 and Δ_3 distortions, the differences between the results from the two supercells are about 0.01 Å or smaller. However, for the Δ_2 distortion the difference is large with the largest one about 0.1 Å. In the Δ_2 distortion, the dopant atom is displaced along the [0001] direction. In the 128-atom supercell, the length of

the supercell along the [0001] direction is $c = 10.043$ Å, which is relatively small and results in large differences in the relaxed bond lengths. The bond lengths in the 1− charge state do not show differences (within 0.001 Å) when relaxing from the initial structures of different distortions. Therefore, in Table 1 we only show one set of bond lengths for the 1− charge state. Another observation from Table 1 is that the Δ_1 distortion is close to C_{3v} symmetry (or pseudo-C_{3v}), i.e., the C_1–D bond is significantly longer than the other three C–D bonds, which have similar bond lengths. The Δ_3 distortion is close to C_{2v} symmetry, i.e., the C_0–D bond and C_1–D bond have similar bond lengths, which are shorter than the $C_{2/3}$–D bonds.

As shown in Fig. 5(a), increasing the supercell size gives rise to shallower $\varepsilon(0/-)$ levels. Even though we cannot afford calculations using larger supercells, by analyzing the atomic and electronic structures it is possible to conclude that these p-type dopants are not hydrogenic defects. First, the deep-level defects are associated with large structural distortions as discussed above. The distortions can be quantified by calculating the energy difference between the structures of the neutral and 1− charge states, as shown in Fig. 5(b). The distortion energies in the neutral and 1− charge states are calculated by $E^0(Q^-) - E^0(Q^0)$ and $E^-(Q^0) - E^-(Q^-)$, where Q^0 and Q^- represent the relaxed structures in the neutral and 1− charge states, respectively.[33] For B on the Si sites, the distortion energy can be over 1 eV. Al on Si sites exhibit the smallest distortion energy, which is consistent with results in Fig. 5(a) that Al gives rise to the shallowest $\varepsilon(0/-)$ level.

Figure 6 shows the partial charge density plots of the defect states for B, Al and Ga on Si_{wz} site. It can be seen that B indeed produces the most localized state, while Al produces the most delocalized states. Ga state is between those of B and Al. This trend is also consistent with that on the $\varepsilon(0/-)$ levels. The shallower level corresponds to more delocalized defect state. For all defects, the localization is more prominent along the [0001] direction. Even for Al, the localization can be clearly seen. On the other hand, along the basal (0001) plane, the delocalization is more prominent.

Table 1. Bond lengths between dopant atom (D) and neighboring Si or C atoms in neutral and 1− charge states obtained by using the 128-atom and 400-atom supercells. In neutral charge state, three distortions are shown, namely, Δ_1, Δ_2 and Δ_3, with the exception of B-on-C_{wz}, for which the third distortion is Δ_2'. For C-site dopants, calculations using the 400-atom supercell were not performed. For B-on-Si_{zb}, the Δ_3 distortion using the 400-atom supercell was not found.

	Neutral charge						1− charge	
	Δ_1 distortion		Δ_2 distortion		Δ_3 distortion			
	128-atom	400-atom	128-atom	400-atom	128-atom	400-atom	128-atom	400-atom
B-on-C_{wz}								
Si_1–D	1.999		1.913		1.948	(Δ_2')	1.897	
$Si_{2/3}$–D	1.930		1.913		1.948	(Δ_2')	1.897	
Si_0–D	1.931		2.029		1.929	(Δ_2')	1.920	
B-on-C_{zb}								
Si_1–D	2.009		1.919		1.913		1.900	
$Si_{2/3}$–D	1.927		1.919		1.973		1.900	
Si_0–D	1.915		2.015		1.915		1.901	
B-on-Si_{wz}								
C_1–D	2.373	2.377	1.657	1.651	1.727	1.724	1.761	1.758
$C_{2/3}$–D	1.657	1.653	1.657	1.651	1.792	1.787	1.761	1.757
C_0–D	1.664	1.661	2.368	2.417	1.742	1.737	1.781	1.772
B-on-Si_{zb}								
C_1–D	2.403	2.392	1.661	1.651	1.724	unfound	1.761	1.756
$C_{2/3}$–D	1.652	1.650	1.661	1.651	1.795	unfound	1.761	1.755
C_0–D	1.647	1.650	2.302	2.400	1.716	unfound	1.752	1.756
Al-on-Si_{wz}								
C_1–D	2.022	2.019	1.964	1.979	1.955	1.958	1.971	1.972
$C_{2/3}$–D	1.965	1.966	1.964	1.979	1.997	1.995	1.971	1.972
C_0–D	1.966	1.963	2.008	1.968	1.967	1.964	1.984	1.980
Al-on-Si_{zb}								
C_1–D	2.022	2.017	1.964	1.976	1.955	1.958	1.971	1.972
$C_{2/3}$–D	1.966	1.967	1.964	1.976	1.997	1.994	1.971	1.972
C_0–D	1.962	1.965	2.007	1.973	1.962	1.966	1.979	1.982
Ga-on-Si_{wz}								
C_1–D	2.077	2.087	1.979	2.003	1.967	1.969	1.992	1.993
$C_{2/3}$–D	1.979	1.977	1.979	2.003	2.028	2.029	1.992	1.993
C_0–D	1.977	1.972	2.043	1.980	1.978	1.974	2.004	2.001
Ga-on-Si_{zb}								
C_1–D	2.077	2.083	1.980	2.004	1.968	1.969	1.994	1.994
$C_{2/3}$–D	1.979	1.977	1.980	2.004	2.029	2.028	1.994	1.995
C_0–D	1.965	1.968	2.036	1.975	1.965	1.970	1.990	1.996

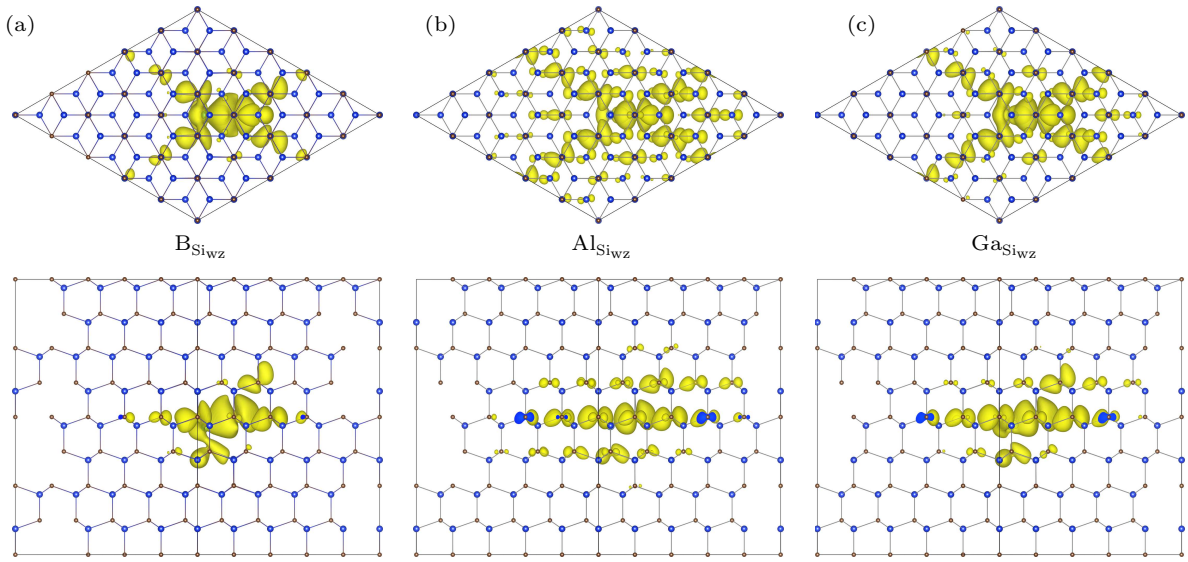


Fig. 6. Partial charge density plots of the defect state in band gap for (a) B, (b) Al, and (c) Ga on Si_{wz} site.

4. Conclusion

We carried out a first-principles study on B, Al and Ga doping in 4H-SiC based on HSE hybrid functional. We determined the occupation preference between the Si and C sites and between the wurtzite-like and zincblende-like sites. B could occupy either the Si or C sites depending on the growth condition, while Al and Ga highly prefer the Si sites. All the three dopants do not exhibit significant energy difference between the wurtzite-like and zincblende-like sites. The dopant atoms in neutral charge states are typically stabilized in three different off-center distorted structures. One of them preserves the C_{3v} symmetry and another two are reduced to C_s (or C_{1h}) symmetry. One of the C_s structures is close to C_{3v} symmetry and another one is close to C_{2v} symmetry. As a p-type dopant, Al exhibits shallower acceptor level and lower formation energy on Si sites than B and Ga. All the p-type dopants in 4H-SiC are not hydrogenic. Instead, they all exhibit localized defect states and large distortion energies between the neutral and 1− charge states. In the future dopant engineering, how to utilize the metastable distortions that yield shallower acceptor levels might be worth of study.

References

[1] Kimoto T and Cooper J A 2014 *Fundamentals of Silicon Carbide Technology* (Singapore: John Wiley & Sons)
[2] Gorai P, McKinney R W, Haegel N M, Zakutayev A and Stevanovic V 2019 *Energy Environ. Sci.* **12** 3338
[3] Van Daal H J, Knippeneerg W F and Wasscher J D 1963 *J. Phys. Chem. Solids* **24** 109
[4] Amano H, Kito M, Hiramatsu K and Akasaki I 1989 *Jpn J. Appl. Phys.* **28** L2112
[5] Kalish R 1999 *Carbon* **37** 781
[6] Sridhara S G, Devaty R P and Choyke W J 1998 *J. Appl. Phys.* **84** 2963
[7] Monemar B 1974 *Phys. Rev. B* **10** 676
[8] Nakamura S, Kumagai H, Kimoto T and Matsunami H 2002 *Appl. Phys. Lett.* **80** 3355
[9] Dmitriev V A, Irvine K G, Carter C H, Kuznetsov N I and Kalinina E V 1996 *Appl. Phys. Lett.* **68** 229
[10] Qian X, Jiang P Q and Yang R G 2017 *Mater. Today Phys.* **3** 70
[11] Kamatagi M D, Sankeshwar N S and Mulimani B G 2007 *Diamond Related Mater.* **16** 98
[12] Pengelly R S, Wood S M, Milligan J W, Sheppard S T and Pribble W L 2012 *IEEE Trans. Microw. Theory Techn.* **60** 1764
[13] Roschke M and Schwierz F 2001 *IEEE Trans. Electron. Dev.* **48** 1442
[14] Trew R J 1997 *Phys. Stat. Sol. (A)* **162** 409
[15] Lebedev A A 1999 *Semiconductors* **33** 107
[16] Deák P, Aradi B, Gali A and Gerstmann U 2003 *Phys. Stat. Sol. (B)* **235** 139
[17] Aradi B, Deák P, Son N T, Janzén E, Choyke W J and Devaty R P 2001 *Appl. Phys. Lett.* **79** 2746
[18] Zhou P L, Shi R Q, He J F and Zheng S K 2013 *Acta. Phys. Sin.* **62** 233101 (in Chinese)
[19] Miyata M, Hattori S and Hayafuji Y 2009 *Jpn. J. Appl. Phys.* **48** 041301
[20] Petrenko T T and Petrenko T L 2016 *Phys. Rev. B* **93** 165203
[21] Gerstmann U, Gali A, Deák P, Frauenheim T and Overhof H 2004 *Mater. Sci. Forum* **457–460** 711
[22] Sun Y Y, Abtew T A, Zhang P and Zhang S B 2014 *Phys. Rev. B* **90** 165301
[23] Kresse G and Furthmüller J 1996 *Comput. Mater. Sci.* **6** 15
[24] Kresse G and Joubert D 1999 *Phys. Rev. B* **59** 1758
[25] Paier J, Marsman M, Hummer K, Kresse G, Gerber I C and Ángyán J G 2006 *J. Chem. Phys.* **124** 154709
[26] Son N T, Chen W M, Kordina O, Konstantinov A O, Monemar B, Janzén E, Hofman D M, Volm D, Drechsler M and Meyer B K 1995 *Appl. Phys. Lett.* **66** 1074
[27] Volm D, Meyer B K, Hofmann D M, Chen W M, Son N T, Persson C, Lindefelt U, Kordina O, Sörman E, Konstantinov A O, Monemar B and Janzén E 1996 *Phys. Rev. B* **53** 15409
[28] Du M H and Zhang S B 2009 *Phys. Rev. B* **80** 115217
[29] Wu X, Gao W, Chai J, Ming C, Chen M, Zeng H, Zhang P, Zhang S and Sun Y Y 2021 *Sci. China Mater.*
[30] Clark H K and Hoard J L 1943 *J. Am. Chem. Soc.* **65** 2115
[31] Salvador J R, Bilc D, Mahanti S D and Kanatzidis M G 2003 *Angew. Chem. Int. Ed.* **42** 1929
[32] Jeffrey G A and Wu V 1966 *Acta Cryst* **20** 538
[33] Christenson S G, Xie W, Sun Y Y and Zhang S B 2015 *J. Appl. Phys.* **118** 135708